AN OCCLUSION MODEL FOR IMPROVING RENDERING QUALITY OF VIEW

Changjian Zhu[1], Hong Zhang[2], and Li Yu[1]

[1] School of Electron. and Inform. Comm., Huazhong Univ. of Sci. & Tech., Wuhan, China
[2] Department of Math and Computer Science, Guilin Normal College, Guilin, China

ABSTRACT

Scene surface exists some occlusions by mutual occlusions or self-occlusions, and then this phenomenon will serious influences 3D vision technique. We present a signal-processing framework to study occlusions of scene. Our method combines discontinuities and establish a mathematical model of occlusion phenomenon. The influences of occlusion on a scene are derived using Fourier theory. In this manner, spectral support of scene occlusion is analyzed in frequency field. Predictions on the frequency content can then be used to control the sampling and rendering in a scene. This extends previous work that the sampling and rendering to be analyzed and estimated for 3D technique. Extensive experimental evaluation demonstrates that our occlusion analysis method significantly outperform competing algorithms.

Index Terms— Spectrum analysis, image-based rendering, occlusion, sampling, view rendering

1. INTRODUCTION

Occlusion is an important feature of appearance in 3D scene. For instance, trees may cause the occlusions to house on the view position and direction in Fig. 1. Occlusion phenomenon serious influences the light transport and view, and then influences the computer vision applications [1]-[3]. Obviously, the occlusions can lead to high frequencies and discontinuities in a radiance function. However, most current vision algorithms do not explicitly consider occlusions. The primary reason is difficulty in formally analyzing them and very complicated of mathematical analysis of occlusions [4, 5].

Currently, existing techniques for occlusion analysis have studied mathematical model. Such as, Lin *et al.* in [6] used a method of layered depth to quantize the occlusions on scene surface. The layered depth can effectively describes the discontinuities in occlusion surface. Reference [7] also provided segmentation of epipolar plane image (EPI) to study the occlusion and discontinuities. The EPI was segmented in the discontinuities surface, and then the occlusions can be mathematical modeled. The work in [8] presented space-time image sequence to analyze the scene surface occlusions. Mutation of the image sequence exists on the scene occlusions. The above methods were based on an approximate method to de-

Fig. 1. Conceptual illustration of scene occlusion. (a) The scene occlusion. Diagram (b) illustrates scene occlusion with respect to the view position variations.

termine the describing of the occlusions. These efforts have produced an extensive array of interesting results that shed light on various aspects of the problem. In particular, the studying of occlusion applications was shown in [9] to analyze the influences of occlusions on spectral supports of plenoptic function (POF). Zhang *et al.* noted that the scene surface occlusions can broaden the plenoptic spectrum. Further results for a frequency analysis of light transport from Durand *et al.* [10] were investigated to analyze occluded complex scenes. Reference [11] also provided an occlusion model using light ray transport. The authors noted that when an occluder was present in the path of a light ray, the radiance along the light ray can not be propagated through the occluder. In [12], Ramamoorthi *et al.* presented a simpler structure model to represent common shadowing situations, and then using Fourier theory to analyze cast shadows in a scene. Recently, Shidanshidi et al. [13] extended a concept of effective sampling density (ESD) [14]. Measuring the variation of ESD on a scene surface would allow us to study occlusions.

The success of these methods depends on accurate 3D proxies. Generally, the shape of scene occlusions is unknown; little amount of surface occlusion mathematical model is challenging topic from dense range scans for a complex scene [15]. Our approach does not depend on dense accurate geometric information; instead we present a mathematical model of surface occlusions. Our contribution to the existing theory is simplification of occlusions by Fourier theory in a complex scene. Additionally, this method can be applied to study 3D video techniques, such as plenoptic sampling [16]-[20].
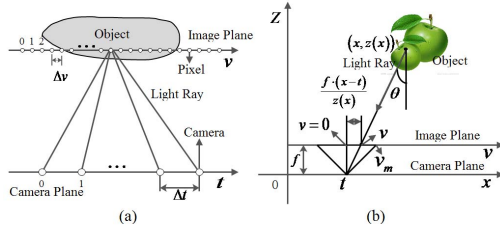
Fig. 2. (a) An illustration of 2D light field. Diagram (b) illustrates an EPI function $p(t,v)$ which describes the relationship between the camera and scene's geometry.

2. STANDARD PARAMETERIZATION

Generally, the light ray can be parameterized using a 7D POF [21, 22]. It can describes the light ray's captured position, viewing direction, the wavelength, and at a certain time in 3D space. In order to reduce the dimensionality, each light ray can be represented using 4D light field/Lumigraph [23, 24]. For simplicity of exposition, and as in [16]-[18], they consider a 2D version of the POF, $p(t,v)$. A visual representation of 2D POF can be constructed if we plot its intensity at all possible (t,v) coordinates as shown in Fig. 2(a). This visual representation is known as the EPI [25]. As shown in Fig. 2(b), a light ray $p(t,v)$ intersects with the object surface at a point with coordinate $(x, z(x))$. The relationship between camera and scene with the EPI of light ray along the x-axis is

$$v = f\tan(\theta), \quad t = x - z(x)v/f. \quad (1)$$

After that, using $l(x,v)$ and under the no self-occlusion assumption we have following expression for a light ray

$$l(x,v) = p(x - z(x)v/f, v), \quad (2)$$

where $\theta = arc\tan(v/f)$, $-v_m \leq v \leq v_m$. And v_m is the maximum of field of view (FOV).

3. MATHEMATICAL MODEL OF SCENE OCCLUSION

Occlusion analysis in 3D scene is a difficult problem because it involves the complex relationship between discontinuous data of scene and view. However, we believe many common occlusion situations have regular structures. As illustrated in Fig. 3, an object is occluded by an occlusion object, where the length of occlusion object is L_2, and the length of occlusion object is L_1. Let $L_2 > L_1$. We define that the center of occlusion object is coordinate origin (i.e., zero coordinate). If the camera is on the left of coordinate origin, then $\theta \in [-\theta_0, \theta_0]$. If the camera is on the right of coordinate origin, then $\theta = [-\theta_1, \theta_2]$, where θ_1 and θ_1 are the max FOV of camera. Here, $\theta = \arctan(v/f)$ and $\theta_1, \theta_2 \leq \theta_0$. Now, the mathematical model of scene occlusion is stated as follows.

Definition 1: Given an occlusion scene, a light ray of camera with respect to position variation can be represented using

$$\Phi(x,v) = \int_{-\theta_1}^{\theta_2} L(x,v)\,O(x,\theta)\,d\theta, \quad (3)$$

where $O(x,\theta) = H_1(x,\theta) + H_2(x,\theta)$.

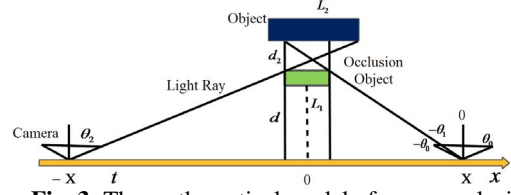Generally, the occlusion is changed as the camera position and direction moving. Therefore, combining the relationship

Fig. 3. The mathematical model of scene occlusion.

between the position and the scene as in Fig. 3, the expressions of $H_1(x,\theta)$ and $H_1(x,\theta)$ are respectively defined as

$$H_1(x,\theta) = \begin{cases} \frac{L_2 - \tan(\theta_2)d_2 + \tan(\theta)d_2}{L_2}, \theta > 0 \\ 1, \theta > \theta_2 \\ 0, \theta \leq 0 \end{cases} \quad (4)$$

$$H_2(x,\theta) = \begin{cases} \frac{L_2 - \tan(|\theta_1|)d_2 + \tan(|\theta|)d_2}{L_2}, \theta < 0 \\ 1, \theta < -\theta_1 \\ 0, \theta \geq 0 \end{cases} \quad (5)$$

where $\tan(\theta) = \frac{|x| - L_1/2}{d}$, and d_2 is the distance between object and occlusion object. The integral results of (3) is given as

$$\begin{aligned} \Phi(x,v) &= \int_{-\theta_1}^{+\theta_2} L(x,v)\,O(x,\theta)\,d\theta \\ &= \int_{-\theta_1}^{+\theta_2} L(x,v)\,\frac{L_2 - \tan(\theta_2)d_2 + \tan(\theta)d_2}{L_2}\,d\theta \\ &= L(x,v) \cdot \int_{-\theta_1}^{+\theta_2} \frac{L_2 - \tan(\theta_2)d_2 + \tan(\theta)d_2}{L_2}\,d\theta \\ &= L(x,v) \cdot O(x,v), \end{aligned} \quad (6)$$

where

$$\begin{aligned} O(x,v) &= \int_{-\theta_1}^{+\theta_2} \frac{L_2 - \tan(\theta_2)d_2 + \tan(\theta)d_2}{L_2}\,d\theta \\ &= \frac{1}{L_2}\left((L_2 - \tan(\theta_2)d_2)(\theta_2 + \theta_1) + d_2 \int_{-\theta_1}^{+\theta_2} \tan(\theta)\,d\theta\right) \\ &= \frac{1}{L_2}\left((L_2 - \tan(\theta_2)d_2)(\theta_2 + \theta_1) + d_2 \frac{cos(\theta_2) + cos(\theta_1)}{\sin(\theta_1) - \sin(\theta_2)}\right) \end{aligned} \quad (7)$$

The above model can provides a commonly occlusion method in a 3D scene. This model consider a small amount of scene geometry information and the camera external parameters.

4. OCCLUSION SPECTRUM IN A 3D SCENE

4.1. Applications

Based on the above quantitative analysis in the occlusion model, a number of important applications can be explored.

3D scene reconstruction for computer vision. Because the assumptions underlying the sampling theory are not fully met in practice, some aliasing is always presented with the reconstruction. To reduce aliasing of the captured images and perfectly reconstruct all of the novel views, the assumption of a band-limited signal is made, and linear interpolation of multi-view images is based on occlusion theory.

Light field rendering. A general data captured is dependent on the scene information for light field rendering, such as texture information, surface shape, occlusion, and so on. With a complex scene, the influence of the scene occlusion on the sampling and the rendering has to be studied.

4.2. Plenoptic Sampling with the Scene Occlusion

In this section, an application of occlusion model to the plenoptic sampling [16]-[18] is given. The purpose is studying the minimum sampling rate of image-based rendering (IBR) data in an occlusion scene.
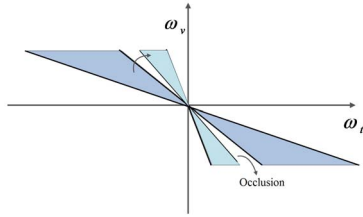
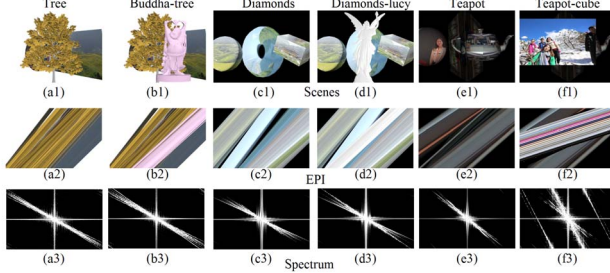**Fig. 4**. The spectral support of POF with the scene occlusion.

Fig. 5. Six synthetic scenes and the corresponding spectral supports. 200 images are uniformly captured for each scene.

4.2.1. Spectrum Parametrization of the Light Field

We assume that the object surface is flat, and non-Lambertian. It can be described using $|z'(x)| < \frac{f}{v_m}$, where $z'(x)$ is the derivative of scene surface z with respect to coordinate x. For a scene with occlusion, its 2D POF spectrum can be stated in the following theorem.

Theorem 1: For a scene, the spectrum of POF can be calculated by the integral for the spectrum of light transport as

$$P(\omega_t, \omega_v) = \int_{-\infty}^{\infty} \tilde{L}_1(x, \omega_v) \exp(-j\omega_t x)\, dx \\ - j2\pi \int_{-\infty}^{\infty} z'(x) \frac{\partial \tilde{L}_1(x,\omega_v)}{f \partial \omega_v} \exp(-j\omega_t x)\, dx, \quad (8)$$

where

$$\tilde{L}_1(x, \omega_v) = \int_{-\infty}^{\infty} l(x, v) \exp(-j(\omega_v - \omega_t z(x)/f)v)\, dv, \quad (9)$$

Proof: Taking the Fourier transform of EPI function $p(t, v)$, we define the plenoptic spectrum expression as [18]

$$P(\omega_t, \omega_v) = \int_{-\infty}^{\infty} \int_{-\infty}^{\infty} p(t, v) e^{-j(\omega_v v + \omega_t t)} dt dv. \quad (10)$$

The integration variables in (10) are changed using (2), and the spectrum of POF can then be given as (8). □

From the above theorem 1, the light transport spectrum $\tilde{L}_1(x, \omega_v)$ can be extracted to independently analyze.

We now present the spectrum of light transport with respect to the occlusion in the following theorem.

Theorem 2: The influence of occlusion on the light transport in frequency domain achieves a convolution function as

$$\Phi(x, \hat{\omega}_v) = \tilde{L}_1(x, \omega_v) \otimes O(x, \omega_v), \quad (11)$$

where

$$O(x, \omega_v) = \int_{-\theta_m}^{\theta_m} O(x, v) \exp(-j\omega_v)\, d\theta. \quad (12)$$

In this case, we consider $\theta_m \to \infty$ due to the finite FOV also cause occlusions when scene object beyond the FOV.

Proof: By the properties of occlusion function, plugging $\Phi(x, v) = l(x, v) \cdot O(x, v)$ back into (9), we obtain
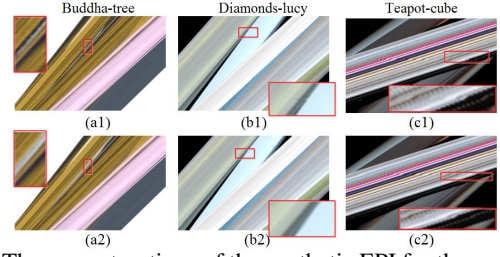

Fig. 6. The reconstructions of the synthetic EPI for three synthetic scenes. (a1)(b1)(c1) The rendered EPI-volumes using USMM. (a2)(b2)(c2) The results by BOCM.

$$\Phi(x, \hat{\omega}_v) = \int_{-\infty}^{\infty} L(x, v) O(x, v) \\ \exp(-j(\omega_v - \omega_t z(x)/f)v)\, dv. \quad (13)$$

The integral results of (13) is given as (11). □

Based on theorem 2, the discontinuity plenoptic spectrums occur because the occlusions. As depicted in Fig. 4, the plenoptic spectrum will be segmented at the occlusion edges because its depths are mutated.

4.2.2. The Bandwidth of Plenoptic Spectrum

In (8), the spectral support of plenoptic spectrums is closely related to occlusion. Additionally, according to (11), the spectral support for the scene is given as

$$(\omega_v + \arg\max(O(x, \omega_v)))\, f \approx \omega_t z(x). \quad (14)$$

By (14), we determine the bandwidth of the POF with respect to the light transport in the following theorem.

Theorem 3: For a occlusion scene, the bandwidth is mainly dependent on ω_v and $\arg\max(O(x, \omega_v))$. The essential bandwidth for this 1D plenoptic spectrum is calculated as

$$BW_v = \{|P(\omega_t, \omega_v)|\} = \{\hat{\omega}_v : |\hat{\omega}_v| \leq \\ \omega_v + \arg\max(O(x, \omega_v)), \text{for } x \in [-\infty, +\infty]\}, \quad (15)$$

For ω_t-axis, the essential bandwidth for this 1D plenoptic spectrum can be calculated as

$$BW_t = \{|P(\omega_t, \omega_v)|\} = \{\hat{\omega}_t : |\hat{\omega}_t| \leq f(\omega_v + \arg\max \\ (O(x, \omega_v))/z(x) + \arg\max(O(x, \omega_v)), \ x \in [-\infty, +\infty]\} \quad (16)$$

where $\hat{\omega}_v$ and $\hat{\omega}_t$ denote frequencies of POF with occlusion.

Using the above bandwidth, let the maximum value of $\hat{\omega}_t$ for the scnee equal to the maximum frequency in the BW_t and obtain,

$$\Omega_t = \frac{f(\omega_v + \arg\max(O(x, \omega_v)))}{\min(z(x))} + \arg\max(O(x, \omega_v)). \quad (17)$$

Similar to Ω_t, let the maximum value of $\hat{\omega}_v$ for the scene equal to the maximum frequency in the BW_v and obtain,

$$\Omega_v = \omega_v + \arg\max(O(x, \omega_v)). \quad (18)$$

4.3. Sampling Theory Based on the Occlusion Model

Using the occlusion model, by (14) and (18), the maximum camera spacing is expressed as

$$\Delta t_{\max} = \frac{z_{\min} \cdot z_{\max}}{f(z_{\max} - z_{\min})(\omega_v + \arg\max(O(x, \omega_v)))}, \quad (19)$$

where $z_{\max}$ is the maximum depth, and $z_{\min}$ the minimum depth. In (19), the camera spacing depends on the depth $z(x)$ and scene occlusion. The camera spacing will be smaller as the scene occlusion becomes more complicated.
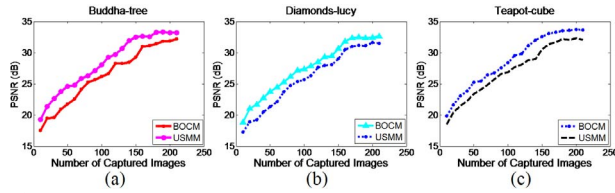
Fig. 7. PSNRs with respect to number of the captured images.

5. EXPERIMENTAL VALIDATION

5.1. Spectral Support Experiments

Inspired by the scene surface occlusion situations, we first synthesize six scenes as depicted in Figs. 5(a1)-(f1). Obviously, each scene exists occlusions, but the occlusions between different scenes are different. In Figs. 5(a1)(a2), when the scene object is a tree which occludes the picture, the EPI-volumes are not parallel. The spectrum of corresponding tree is a region which is shown in Fig. 5(a3). When the scene is a buddha-tree as in Figs. 5(b1), the spectrum is broadened and segmented by the occlusions between the buddha and picture. This phenomenon occurs because the scene occlusions more serious than that of tree scene, as shown in Figs. 5(a1)(b1). Further, the EPI-volumes will be more complicated as shown in Figs. 5(b2)(d2)(f2) and the spectrum of 3D scene will be expanded because of the scene occlusions becomes more complicated. It can be observed in Figs. 5(b3)(d3)(f3)) that the padding between the two diagonal lines of the spectrum is more complicated than that of Figs. 5(a3)(c3)(e3). Therefore, we can determine the relationship between the scene occlusions and spectrum to derive the occlusion model.

5.2. Simulation Experiments

To testify that our proposed method can be applied to analyze the scene occlusions, plenoptic sampling and reconstruction simulation experiments are performed. We present evaluation results on the buddha-tree, diamonds-lucy, and teapot-cube data-sets, as depicted in Figs. 5(b1)(c1)(f1). The sampling theory of the IBR based on the occlusion model (BOCM) in (19) is applied to calculate the plenoptic sampling rates of three synthetic scenes. To evaluate comparison, the minimum sampling rate determination method presented by Chai [16] is selected. This method only uses the minimum depth and the maximum depth (USMM) as $\Delta t_{max} = \frac{z_{min} \cdot z_{max}}{\Omega_v f(z_{max} - z_{min})}$.

Because the assumptions underlying plenoptic sampling theory are not fully met in practice, some aliasing is presented with the reconstruction as shown in Fig. 6 [26]. However, the aliasing of the rendered images in Figs. 6(a2)(b2)(c2) is reduced compared to that of the rendered images in Figs. 6(a1)(b1)(c1). The PSNRs in Figs. 6(a1) and (a2) are 32.28 and 32.76 dB, respectively. The PSNRs in Figs. 6(b1) and (b2) are 31.85 dB and 32.89 dB, respectively. The PSNRs in Figs. 6(c1) and (c2) are 32.39 and 33.63 dB, respectively. The same results can be obtained by Fig. 7 for using different number of captured images to rendering a set of novel views. The PSNRs by the method of BOCM is larger than that of USMM. The reason can be seen by the influence of the occlusion on the rendering quality very obvious. This demonstrates that the proposed method can improve the rendering quality, and the performance of BOCM is better than the USMM.

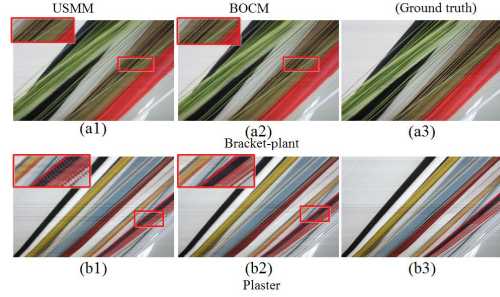Fig. 8. (a) Bracket-plant scene. (b) Plaster scene.

Fig. 9. The reconstructions of EPI for two actual scenes.

5.3. Actual Scenes

To evaluate the proposed occlusion model, the rendering experiments also are carried out using two actual scenes depicted in Figs. 8(a) and (b). The two actual scenes are captured using an camera along a track. The rendering quality of novel views is measured using BOCM and USMM.

For the rendering results, it should be observed in Fig. 9 that the reconstructed views are some obvious ghosting and aliasing either the bracket-plant scene or the plaster scene. Apparently, the rendering quality in Fig. 9(a2) is better than that of in Fig. 9(a1). The ghosting occurs because the scene complexity such as the leafage and irregular shape which are challenging reconstructed accurately. However, when using the proposed occlusion model, the ghosting and aliasing in the rendered views will decreases. There are the same phenomenon between Fig. 9(b2) and Fig. 9(b1). The PSNRs in Figs. 9(a1) and (a2) are 31.47 and 32.05 dB, respectively. The PSNRs in Figs. 9(b1) and (b2) are 30.78 and 31.96 dB, respectively. These results also leads to the thinking that the proposed occlusion model can be applied to analyze complex scene for estimating minimum sampling rate of IBR.

6. CONCLUSION

In this paper, we have proposed a scene occlusion model using the Fourier theory. This occlusion model has been studied, and its spectrum is presented. The influence of the scene occlusion on the spectrum has been studied along both the image plane and camera plane frequency axis. Based on the support of the spectrum, the spacing between the cameras needed to reconstruct the continuous light field up to a certain camera plane frequency has been determined in the IBR.

7. ACKNOWLEDGMENTS

8. REFERENCES

[1] J. Carranze, C. Theobolt, M. A. Magnor, and H. P. Seidel, "Freeviewpoint video of human actors," in *Proc. Annu. Conf. Comput. Graph,* Jul. 2003, pp. 569-577.

[2] T. Maugey, and P. Frossard, "Interactive multiview video system with low complexity 2D look around at decoder," *IEEE Trans. on Multimedia,* vol. 15, no. 5, pp. 1070-1082, 2013.

[3] L. HanShin, and P. HyunWook, "An efficient multi-view generation method from a single-view video based on affine geometry information," *IEEE Trans. on Multimedia,* vol. 16, no. 3, pp. 726-737, 2014.

[4] M. Levoy, "Light fields and computational imaging," *IEEE Computer,* vol. 8, pp. 46-55, 2006.

[5] J. Berent, and P. L. Dragotti, "Plenoptic manifolds," *IEEE. Signal Processing Magazine,* vol. 24, no. 6, pp. 34-44, Nov. 2007.

[6] M. Lin and C. Tomasi, "Surfaces with occlusions from layered stereo," in *Proc. IEEE Conf. Comput. Vision and Pattern Recognition,* 2003, pp. 710-717.

[7] J. Berent and P.L. Dragotti, "Segmentation of epipolar plane image volumes with occlusion and dissocclusion competition," in *Proc. IEEE Int. Workshop Multimedia Signal Processing,* Oct. 2006, pp. 182-185.

[8] M. Ristivojevic and J. Konrad, "Space-time image sequence analysis: Object tunnels and occlusion volumes," *IEEE Trans. Image Processing,* vol. 15, pp. 364-376, 2006.

[9] C. Zhang and T. Chen, "Spectral analysis for sampling image-based rendering data," *IEEE Trans. Circuits Syst. Video Technol.,* vol. 13, no. 11, pp. 1038-1050, 2003.

[10] F. Durand, N. Holzschuch, C. Soler, E. Chan, and F. X. Sillion, "A frequency analysis of light transport," *ACM Trans. on Graphics,* vol.24, no.3, pp. 1115-1126, 2005.

[11] C. K. Liang, Y. C. Shih, and H. H. Chen, "Light field analysis for modeling image formation," *IEEE Trans. on Image Process.,* vol. 20, no. 2, pp. 446-460, 2011.

[12] R. Ramamoorthi, M. Koudelka, and P. Belhumeur, "A fourier theory for cast shadows," *IEEE Trans. on Pattern Analysis and Machine Intelligence,* vol. 27, no.2, pp. 288-295, 2005.

[13] H. Shidanshidi, F. Safaei, and W. Li, "Estimation of signal distortion using effective sampling density for light field-based free viewpoint video," *IEEE Trans. on Multimedia,* vol. 17, no. 10, pp. 1677-1693, 2015.

[14] H. Shidanshidi, F. Safaei, and W. Li, "Objective evaluation of light field rendering methods using effective sampling density," in *Proc. 13th MMSP,* Hangzhou, Oct. 2011, pp. 1-6.

[15] G. Chaurasia, O. Sorkine-Hornung, and G. Drettakis, "Silhouette-aware warping for image-based rendering," in *Proc. of Computer Graphics Forum,* vol. 30, no. 4, 2011, pp. 1223-1232.

[16] J.-X. Chai, X. Tong, S.-C. Chan, and H.-Y. Shum, "Plenoptic sampling," in *Proc. SIGGRAPH,* New York, NY, USA, 2000, pp. 307-318.

[17] M. N. Do, D. Marchand-Maillet, and M. Vetterli, "On the bandwidth of the plenoptic function," *IEEE Trans. Image Process.,* vol. 21, no. 2, pp. 708-717, Feb. 2012.

[18] C. Gilliam, P. Dragotti, and M. Brookes, "On the spectrum of the plenoptic function," *IEEE Trans. Image Process.,* vol. 23, no. 2, pp. 502-516, Feb. 2014.

[19] C. Zhu, L. Yu, Z. Yan, and S. Xiang, "Frequency estimation of the plenoptic function using the autocorrelation theorem," *IEEE Trans. on Computational Imaging,* Feb. 2017.

[20] C. J. Zhu, and L. Yu, "Spectral analysis of image-based rendering data with scene geometry," *Multimedia Systems,* 1-18, 2016.

[21] E. H. Adelson, and J. R. Bergen, "The plenoptic function and the elements of early vision," in *Computational Models of Visual Processing.* Cambridge, MA, USA: MIT Press, 1991, pp. 3-20.

[22] L. McMillan, and G. Bishop, "Plenoptic modeling: An image-based rendering system," in *Computer Graphics (SIGGRAPH'95),* Aug. 1995, pp. 39-46.

[23] S. Gortler, R. Grzeszczuk, R. Szeliski, and M. Cohen, "The lumigraph," in *Proc. SIGGRAPH,* 1996, pp. 43-54.

[24] M. Levoy, and P. Hanrahan, "Light field rendering," in *Proc. SIGGRAPH,* New Orleans, USA, 1996, pp. 31-40.

[25] R. Bolles, H. Baker, and D. Marimont, "Epipolar-plane image analysis: An approach to determining structure from motion," *Int. J. Comput. Vis.,* vol. 1, no. 1, pp. 7-55, 1987.

[26] C. Buehler, M. Bosse, L. McMillan, S. J. Gortler, and M. F. Cohen, "Unstructured lumigraph rendering," In: *Proc. SIGGRAPH,* 2001, pp. 425-432.